# Analytic and numerical study of two-frequency undulator radiation

F. Ciocci, G. Dattoli, L. Giannessi, A. Torre, and G. Voykov
*Comitato Nazionale per la Ricerca e per lo Sviluppo dell'Energia Nucleare e delle Energie Alternative, Area Innovazione, Dipartimento Sviluppo Tecnologie di Punta, Centro Ricerche Energia Frascati, Casella Postale 65-00044 Frascati, Roma, Italy*
(Received 14 September 1992)

In this paper we discuss the spectroscopic details of the two-frequency undulator, a recently proposed device to suppress the sideband instability in free-electron lasers. We present an analytic and numerical approach to the problem and discuss the intrinsic differences between the brightnesses of one- and two-frequency undulators. We study the dependence of the emission on various physical parameters including the electron-beam qualities.

PACS number(s): 41.60.Cr, 41.85.Lc, 52.75.Ms, 07.77.+p

## I. INTRODUCTION

In a recent paper, Iracane and Bamas [1], have proposed a two-frequency undulator (TFU) and have shown that such a device generates a laser field having both a large extraction efficiency and a narrower spectrum. The spectral features of the radiation, emitted by a relativistic electron moving in a TFU, share some analogies with the rather complicated recently discussed "spectroscopic" pattern of undulator radiation when the effects of both undulator and betatron motion are included in the analysis [2]. In this paper we use the concepts and mathematical tools exploited in Ref. [2] to discuss the details of TFU spectroscopy.

The paper contains four sections. In Sec. II we discuss an analytic approach to the problem. Section III is devoted to a fully numerical investigation and comparison with the analytical results. Finally, Sec. IV contains concluding remarks and comments relevant to the modification induced in the spectrum by a nonzero energy spread of the electron beam.

## II. TFU SPECTROSCOPY: AN ANALYTIC APPROACH

In the following we consider the electron motion induced on a relativistic electron by a plane undulator exhibiting the following on-axis field:

$$\mathbf{B}\equiv B_0(0,b(z),0)\ ,\qquad b(z)=a_1\sin(k_u^{(1)}z)+a_2\sin(k_u^{(2)}z)\ ,\quad k_u^{(\alpha)}=\frac{2\pi}{\lambda_u^{(\alpha)}}\ . \tag{1}$$

The electron's equation of motion will therefore be provided by

$$\frac{d}{dt}v_x=\frac{e}{c}\frac{B_0}{m_0\gamma}v_z[a_1\sin(k_u^{(1)}z)+a_2\sin(k_u^{(2)}z)]\ ,$$
$$\frac{d}{dt}v_z=-\frac{eB_0}{cm_0\gamma}v_x[a_1\sin(k_u^{(1)}z)+a_2\sin(k_u^{(2)}z)]\ . \tag{2a}$$

Furthermore,

$$\dot z^2=\beta^2c^2\left[1-\frac{\beta_x^2}{\beta^2}\right]\ . \tag{2b}$$

The first of Eqs. (2a) is easily integrated, thus yielding

$$v_x=-c\frac{K}{\gamma}[a_1\cos(k_u^{(1)}z)+\tilde r a_2\cos(k_u^{(2)}z)]\ , \tag{3}$$

where

$$K=\frac{eB_0\lambda_u^{(1)}}{2\pi m_0c^2}\ ,\quad \tilde r=\frac{\lambda_u^{(2)}}{\lambda_u^{(1)}}\ , \tag{4}$$

and the fact that we have defined $K$ in terms of the period $\lambda_u^{(1)}$ implicitly suggests that we are assuming that "mode" as the carrier. The longitudinal velocity can be derived from Eq. (2b), and in the hypothesis of ultrarelativistic motion, thus retaining the $1/2\gamma^2$ contributions only, we find

$$\dot z\cong\beta^*c-\frac{K^2c}{4\gamma^2}\{a_1^2\cos(2\omega_u^{(1)}t)+\tilde r^2a_2^2\cos(2\omega_u^{(2)}t)+2\tilde r a_1a_2[\cos(\Delta_+t)+\cos(\Delta_-t)]\}\ , \tag{5}$$

where

$$\beta^*=\left[1-\frac{1}{2\gamma^2}\left[1+\frac{K^{*2}}{2}\right]\right]\ ,\qquad K^{*2}=K^2(a_1^2+\tilde r^2a_2^2)\ , \tag{6a}$$

and

$$\omega_u^{(\alpha)}=\frac{2\pi c}{\lambda_u^{(\alpha)}}\ ,\quad \Delta_\pm=\omega_u^{(1)}\pm\omega_u^{(2)}\ . \tag{6b}$$

The equations of motion therefore yield straightforwardly the electron trajectory, namely

 

$$x \cong -\frac{c}{\omega_u^{(1)}}\frac{K}{\gamma}[a_1 \sin(\omega_u^{(1)}t)+\tilde{r}^2 a_2 \sin(\omega_u^{(2)}t)] ,$$

$$y=0 , \tag{7}$$

$$z \cong \beta^* ct - \frac{c}{\omega_u^{(1)}}\frac{K^2}{8\gamma^2}\left[a_1^2 \sin(2\omega_u^{(1)}t) + \tilde{r}^3 a_2^2 \sin(2\omega_u^{(2)}t) + 4\tilde{r}^2 a_1 a_2 \times \left[\frac{1}{(\tilde{r}+1)}\sin(\Delta_+ t) + \frac{1}{(\tilde{r}-1)}\sin(\Delta_- t)\right]\right] .$$

The next step will be the evaluation of the radiation integral [3], namely

$$\frac{d^2 I}{d\omega d\Omega} = \frac{e^2\omega^2}{4\pi^2 c}\sum_{\alpha=x,y,z}\left|\int_0^T E_\alpha(t)dt\right|^2 , \tag{8}$$

where

$$E_\alpha = [\mathbf{n}\times(\mathbf{n}\times\boldsymbol{\beta})]_\alpha \exp\left[i\omega\left[t-\frac{\mathbf{n}\cdot\mathbf{r}}{c}\right]\right] \quad (\alpha=x,y,z) \tag{9}$$

and

$$\mathbf{n} \equiv (\psi\cos\varphi, \psi\sin\varphi, 1-\tfrac{1}{2}\psi^2) , \tag{10}$$

and thus

$$\mathbf{n}\cdot\mathbf{r} \simeq -\frac{c}{\omega_u^{(1)}}\frac{K}{\gamma}\psi\cos\varphi F_x(t) + (1-\tfrac{1}{2}\psi^2)\beta^* ct - \frac{c}{\omega_u^{(1)}}\frac{K^2}{8\gamma^2}F_z(t) . \tag{11}$$

Recall that $\psi$ is of the order of $\gamma^{-1}$. The $F(t)$ components are defined below:

$$\begin{aligned} F_x(t) &= a_1 \sin(\omega_u^{(1)}t)+\tilde{r}^2 a_2 \sin(\omega_u^{(2)}t) , \\ F_z(t) &= a_1^2 \sin(2\omega_u^{(1)}t)+\tilde{r}^3 a_2^2 \sin(2\omega_u^{(2)}t) \\ &\quad + 4\tilde{r}^2 a_1 a_2\left[\frac{1}{1+\tilde{r}}\sin(\Delta_+ t)-\frac{1}{1-\tilde{r}}\sin(\Delta_- t)\right] . \end{aligned} \tag{12}$$

The exponential in Eq. (8) can be written in terms of Bessel function expansion as follows:

$$\exp\left[i\frac{\omega}{2\gamma^2}\left[1+\frac{K^{*2}}{2}+\gamma^2\psi^2\right]t\right] \times \sum_{l=-\infty}^{+\infty}\sum_{r=-\infty}^{+\infty} e^{-i(l\omega_u^{(1)}+r\Delta_-)t} J_l(Z_\omega^{(1)}, \xi_\omega^{(1)}) \times J_r(A_\omega^-) \sum_{m=-\infty}^{+\infty}\sum_{s=-\infty}^{+\infty} e^{-i(m\omega_u^{(2)}+s\Delta_+)t} \times J_m(Z_\omega^{(2)}, \xi_\omega^{(2)}) J_s(A_\omega^{(+)}) , \tag{13}$$

where

$$\begin{aligned} Z_\omega^{(1)} &= -\frac{\omega}{\omega_u^{(1)}}\frac{a_1 K}{\gamma}\psi\cos\varphi , \\ \xi_\omega^{(1)} &= -\frac{\omega}{\omega_u^{(1)}}\frac{a_1^2 K^2}{8\gamma^2} , \\ Z_\omega^{(2)} &= -\frac{\omega}{\omega_u^{(1)}}\frac{\tilde{r}^2 a_2 K}{\gamma}\psi\cos\varphi , \\ \xi_\omega^{(2)} &= -\frac{\omega}{\omega_u^{(1)}}\frac{\tilde{r}^3 a_2^2 K^2}{8\gamma^2} , \\ A_\omega^{(+)} &= -\frac{\omega}{\omega_u^{(1)}}\frac{4\tilde{r}^2 a_1 a_2}{1+\tilde{r}}\frac{K^2}{8\gamma^2} , \\ A_\omega^{(-)} &= +\frac{\omega}{\omega_u^{(1)}}\frac{4\tilde{r}^2 a_1 a_2}{1-\tilde{r}}\frac{K^2}{8\gamma^2} , \end{aligned} \tag{14}$$

and $J_n(x,y)$ are two variables generalized Bessel functions discussed in the following. The cross products in Eq. (9) are explicitly given by

$$\begin{aligned} [\mathbf{n}\times(\mathbf{n}\times\boldsymbol{\beta})]_x &\cong \psi\cos\varphi + \frac{K}{\gamma}[a_1\cos(\omega_u^{(1)}t) + \tilde{r}a_2\cos(\omega_u^{(2)}t)] , \\ [\mathbf{n}\times(\mathbf{n}\times\boldsymbol{\beta})]_y &\cong \psi\sin\varphi , \\ [\mathbf{n}\times(\mathbf{n}\times\boldsymbol{\beta})]_z &\cong -\frac{K}{\gamma}\psi\cos\varphi[a_1\cos(\omega_u^{(1)}t) + \tilde{r}a_2\cos(\omega_u^{(2)}t)] - \psi^2 , \end{aligned} \tag{15}$$

and the explicit form of $E_\alpha$ is reported below:

$$E_x = \sum_l\sum_r\sum_m\sum_s \exp\left\{i\left[\frac{\omega}{2\gamma^2}\left[1+\frac{K^{*2}}{2}+\gamma^2\psi^2\right]-(l\omega_u^{(1)}+r\Delta_-+m\omega_u^{(2)}+s\Delta_+)\right]t\right\} \times \left[\psi\cos\varphi J_{l,r,m,s} + \frac{K}{2\gamma}[a_1(J_{l-1,r,m,s}+J_{l+1,r,m,s})+\tilde{r}a_2(J_{l,r,m-1,s}+J_{l,r,m+1,s})]\right] ,$$

$$E_y = \psi\sin\varphi\sum_l\sum_r\sum_m\sum_s \exp\left\{i\left[\frac{\omega}{2\gamma^2}\left[1+\frac{K^{*2}}{2}+\gamma^2\psi^2\right]-(l\omega_u^{(1)}+r\Delta_-+m\omega_u^{(2)}+s\Delta_+)\right]t\right\} J_{l,r,m,s} , \tag{16}$$

$$E_z=-\sum_l\sum_r\sum_m\sum_s \exp\left\{i\left[\frac{\omega}{2\gamma^2}\left[1+\frac{K^{*2}}{2}+\gamma^2\psi^2\right]-(l\omega_u^{(1)}+r\Delta_-+m\omega_u^{(2)}+s\Delta_+)\right]t\right\}$$
$$\times\left[\psi^2 J_{l,r,m,s}+\psi\cos\varphi\frac{K}{2\gamma}[a_1(J_{l+1,r,m,s}+J_{l-1,r,m,s})+\tilde{r}a_2(J_{l,r,m+1,s}+J_{l,r,m-1,s})]\right],$$

The symbol $J_{l,r,m,s}$ denotes the following product of Bessel functions:

$$J_{l,r,m,s}=J_l(Z_\omega^{(1)},\xi_\omega^{(1)})J_r(A_\omega^{(-)})J_m(Z_\omega^{(2)},\xi_\omega^{(2)})J_s(A_\omega^{(+)}) . \tag{17}$$

The above result confirms how complicated the spectroscopic pattern of a TFU is. To simplify the problem, we limit the analysis to the on-axis radiated brightness ($\psi=0$). In this case the only surviving component is $E_x$, which yields

$$\left.\frac{d^2I}{d\omega d\Omega}\right|_{\psi=0}=\frac{e^2}{4\pi^2c}(\omega T)^2\left[\left[\sum_l\sum_r\sum_m\sum_s B_{l,r,m,s},\frac{\sin(\varphi_{l,r,m,s}T)}{\varphi_{l,r,m,s}T}\right]^2\right.$$
$$\left.+\left[\sum_l\sum_r\sum_m\sum_s B_{l,r,m,s}\frac{1-\cos(\varphi_{l,r,m,s}T)}{\varphi_{l,r,m,s}T}\right]^2\right], \tag{18}$$

where we have defined

$$\varphi_{l,r,m,s}=\frac{\omega}{2\gamma^2}\left[1+\frac{K^{*2}}{2}\right]-(l\omega_u^{(1)}+r\Delta_-+m\omega_u^{(2)}+s\Delta_+) ,$$
$$B_{l,r,m,s}=\frac{K}{2\gamma}[a_1(J_{l+1,r,m,s}+J_{l-1,r,m,s})+\tilde{r}a_2(J_{l,r,m+1,s}+J_{l,r,m-1,s})] , \tag{19}$$

and

$$T=\frac{L_u}{c} , \tag{20}$$

with $L_u$ being the total undulator length. The first indication we obtain from Eq. (18) is that the peaks of the various harmonics are centered at

$$\omega=2\gamma^2\frac{l\omega_u^{(1)}+r\Delta_-+m\omega_u^{(2)}+s\Delta_+}{\left[1+\frac{K^{*2}}{2}\right]} . \tag{21}$$

To understand properly the spectroscopic characteristics of the TFU, we should specify a number of rules which may help to understand the emission and the harmonic selection mechanisms.

Before getting into more specific details, it is worth recalling some of the properties of the two-variable generalized Bessel functions, namely [2]

$$J_n(x,y)=\sum_{l=-\infty}^{+\infty}J_{n-2l}(x)J_l(y) \tag{22}$$

and

$$J_n(x,0)=J_n(x) ,$$
$$J_n(0,y)=\begin{cases}J_{n/2}(y) , & n \text{ even}\\ 0 , & n \text{ odd}\end{cases} . \tag{23}$$

On axis $Z_\omega^{(1)}=Z_\omega^{(2)}=0$; according to (23), we find that

$$J_{l\pm1,r,m,s}\neq0 \text{ for } l \text{ odd and } m \text{ even} , \tag{24a}$$
$$J_{l,r,m\pm1,s}\neq0 \text{ for } l \text{ even and } m \text{ odd} . \tag{24b}$$

As a consequence, $J_{l\pm1,r,m,s}=J_{l,r,m\pm1,s}=0$ for $(l+m)$ even. The problem is now that of combining the various "quantum" numbers to specify the line structure. We go back to Eq. (22) and write

$$l\omega_u^{(1)}+r\Delta_-+m\omega_u^{(2)}+s\Delta_+=p\omega_u^{(1)}+(r+q)\Delta_- . \tag{25}$$

This arrangement means that we have introduced a prin-

TABLE I. "Quantum" numbers and harmonic selections in a TFU.

| $p$ | $s$ | $q$ | $l$ | $m$ | $(l+s)\omega_u^{(1)}+(m+s)\omega_u^{(2)}$ |
|---|---|---|---|---|---|
| 1 | 1 | −1 | −1 | 0 | $\omega_u^{(1)}+(r-1)\Delta_-$ |
| 1 | 1 | 0 | 0 | −1 | $\omega_u^{(1)}+r\Delta_-$ |
| 1 | 1 | 1 | 1 | −2 | $\omega_u^{(1)}+(r+1)\Delta_-$ |
| 1 | 0 | −1 | 0 | 1 | $\omega_u^{(1)}+(r-1)\Delta_-$ |
| 1 | 0 | 0 | 1 | 0 | $\omega_u^{(1)}+r\Delta_-$ |
| 1 | 0 | 1 | 2 | −1 | $\omega_u^{(1)}+(r+1)\Delta_-$ |
| 1 | −1 | −1 | 1 | 2 | $\omega_u^{(1)}+(r-1)\Delta_-$ |
| 1 | −1 | 0 | 2 | 1 | $\omega_u^{(1)}+r\Delta_-$ |
| 1 | −1 | 1 | 3 | 0 | $\omega_u^{(1)}+(r+1)\Delta_-$ |

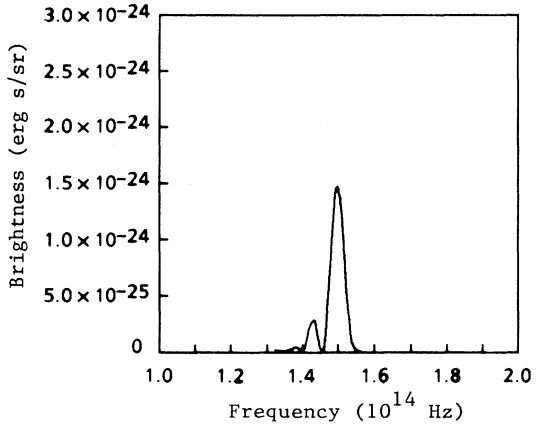


FIG. 1. TFU brightness vs frequency, analytical computation keeping contributions of $r$ harmonics from $-1$ to $+1$ (parameters: $K=1$, $\lambda_u^{(1)}=5$ cm, $\lambda_u^{(2)}=5.155$, $L_u=166.7$ cm, $\gamma=54.772$, $a_1=1$, $a_2=0.1819$).

cipal number $p$, defining the center of the line. The number $r$ specifies the subharmonic structure, and finally $q$ accounts for the contribution of the nearest harmonic. This last point can be better understood by noticing that

$$(l+s)\omega_u^{(1)}+(m+s)\omega_u^{(2)}=(p+q)\omega_u^{(1)}-q\omega_u^{(2)} . \quad (26)$$

The selection rules (24a) and (24b) allow us to fix the various combinations as indicated by Table I. From the table it follows that the line having $p=1$, has a further substructure provided by the $r$ and $q$ contributions. The numerical handling of the above results is shown in Figs. (1–3), where the importance of the $r$ contribution is stressed. The brightness is indeed plotted for $p=1$, keeping increasing contributions of $r$. The line shape *does not change significantly,* keeping further contributions with $|r|>6$. The comparison of the above analysis with a fully numerical treatment will be accomplished in the next section.

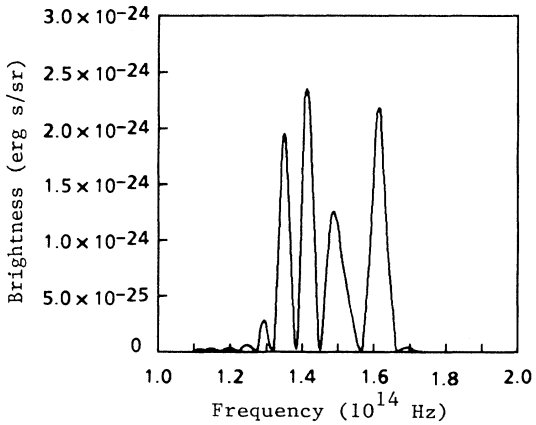


FIG. 2. Same as in Fig. 1 and $-3\le r\le 3$.

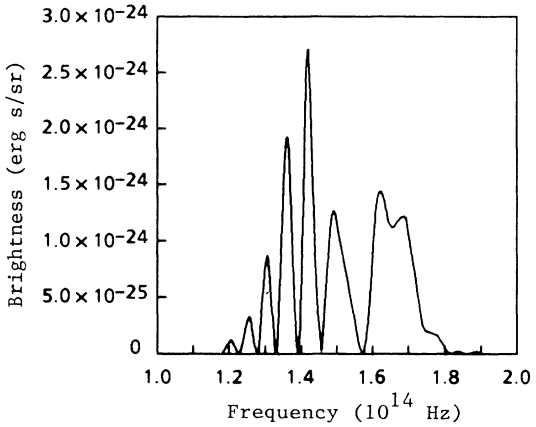


FIG. 3. Same as in Fig. 1 and $-6\le r\le 6$.

## III. NUMERICAL ANALYSIS AND COMPARISON WITH ANALYTICAL RESULTS

In this section we present the results of a fully numerical integration of the TFU problem and the comparison with the analysis developed in the previous section.

The numerical integration of (8) has been accomplished using both the analytical trajectory and that derived by solving numerically the Lorentz equation by means of the initial value problem algorithm. For the ranges of electron-beam energies considered, the two methods did not provide significant differences. The numerical integration of the Lienard-Wiechert integral has been accomplished using an adaptive algorithm (described in Ref. [4]) requiring a relative error of the order of $10^{-8}$. The result of the numerical analysis is shown in Fig. 4, where the dotted line is the result of the integration with the Bessel-function method and the important conclusion

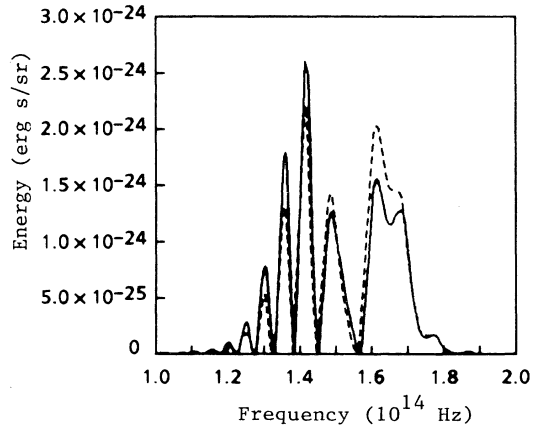


FIG. 4. TFU brightness vs frequency (same parameters as in Fig. 1). Solid line, numerical; dashed line, analytical, keeping contributions $p=1$, $q=0$, $-1\le s\le 1$, $-12\le r\le 12$. The case $p=1$, $-1\le q\le 1$, $-1\le s\le 1$, $-12\le r\le 12$ is almost indistinguishable from the fully numerical calculations.

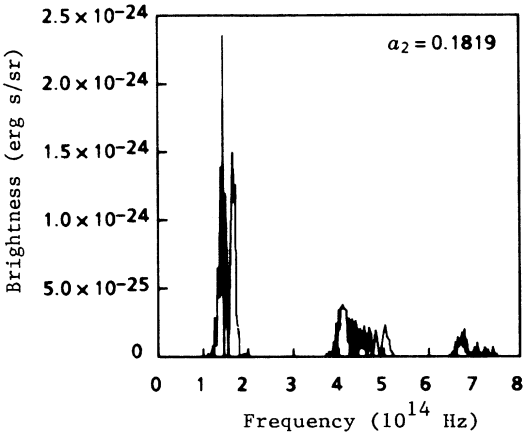


FIG. 5. TFU brightness for a larger-frequency domain. Same parameters as in Fig. 1.

is that the analysis of Sec. II, with its relevant physical interpretation, is fully reliable. We have already stressed that the difference with respect to the case of the "one-frequency undulator" (OFU) is that, e.g., the first harmonic splits in a number of subpeaks, determined by the number $r$. The width of each subpeak is

$$\Delta\omega \cong \frac{\gamma^2}{(1+K^{*2}/2)} \frac{\omega_u^{(1)}}{N} , \tag{27}$$

which is essentially the width of the OFU line. The above relation does not include the effect of the interference. The "macrostructure" of the TFU line is presumably due to the form factor induced by the $J_r(A_\omega^{(-)})$ function. This point will be commented on in the concluding remarks.

A more complete view to the emission scenario is offered by Fig. 5, where the first, third, and fifth harmonic brightnesses have been plotted for $K=1$. The higher harmonic peaks are substantially suppressed with respect to the fundamental. In agreement with the OFU case, no second harmonic is radiated on axis. This is, however, not a general feature of the TFU brightness, as we will discuss in the next section.

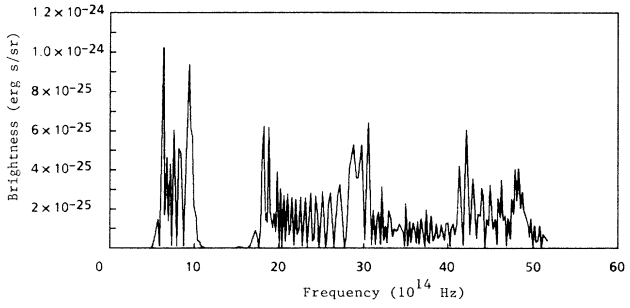


FIG. 6. TFU brightness vs frequency (same parameters as in Fig. 1 but $K=2$).

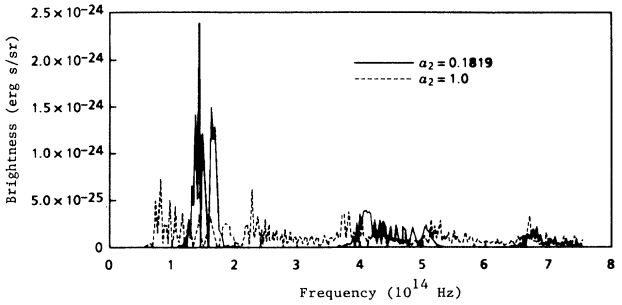


FIG. 7. TFU brightness vs frequency for different values of the amplitudes $a_2$ (same parameters as in Fig. 1).

## IV. CONCLUDING REMARKS

In the previous sections we have presented a rather detailed analysis of the TFU spectroscopy. The results we have obtained have indicated that TFU and OFU brightness exhibit significant differences but still share important analogies, such as the absence of even on-axis harmonics and a distinct set of odd harmonics. We have stressed that this is not a general rule. A first example is provided by Fig. 6, where the on-axis brightness is plotted versus the frequency for $K=2$. It is evident that the first-harmonic line is separated, while the spectrum from the third to the seventh harmonics is a quasicontinuum. Such a "strange" behavior is further supported by Fig. 7, where the brightness is plotted for $K=1$ in the cases of $a_2 \ll a_1$ and $a_2 = a_1$. In the second hypothesis, it is evident that the peaks are substantially suppressed and that radiation can be found almost everywhere, including the forbidden regions of the OFU regime. It is premature to speculate about the possible applications of this effect; it seems, however, that interesting possibilities, like that of operating on a continuous band, are open.

A point not yet touched on is that relevant to the

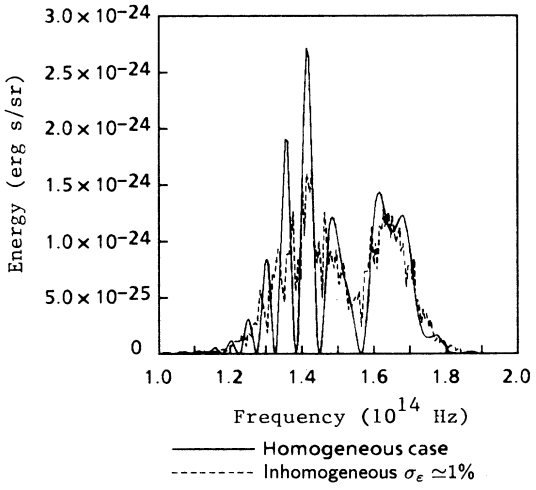


FIG. 8. TFU brightness vs frequency homogeneous and inhomogeneous cases (same parameters as in Fig. 1).

broadening of the emission line induced by the beam energy spread. Such a problem deserves a deeper analysis, mainly in connection with the possible use of the TFU in FEL experiments.

In Fig. 8 we show the result of the integration for a beam having an energy spread of 1%. The effect on the brightness is what one qualitatively expects: there is indeed a reduction and a broadening of the various lines with a consequent "smoothing" of the structure induced by the $r$-harmonics component.

This paper has been devoted to a preliminary analysis of the characteristics of the TFU brightness. It was essentially aimed at showing how many interesting features it displays. A more detailed study will be presented in a future publication, where the importance of the device for FEL operation will also be discussed.

[1] D. Iracane and P. Bamas, Phys. Rev. Lett. **67**, 3086 (1991).
[2] G. Dattoli, L. Giannessi, M. Richetta, and A. Torre, Phys. Rev. A **45**, 4023 (1992).
[3] J. D. Jackson, *Classical Electrodynamics* (Wiley, New York, 1962).
[4] G. E. Forsythe, M. A. Malcolm, and C. B. Moler, *Computer Methods for Mathematical Computations* (Prentice-Hall, Englewood Cliffs, NJ, 1977).